Received: 19 May 2022 | Revised: 16 August 2022 | Accepted: 11 October 2022

IET Power Electronics

DOI: 10.1049/pel2.12411

The Institution of Engineering and Technology WILEY

ORIGINAL RESEARCH

Improvement of two grid power factor control methods for matrix converter open-end-winding drive with common-mode voltage elimination supplied by unbalanced grid

Luka Stanić[1] | **Leposava Ristić**[1] | **Milan Bebić**[1] | **Marco Rivera**[1,2]

[1]Department of Power Converters and Drives, School of Electrical Engineering, University of Belgrade, Belgrade, Serbia

[2]Department of Electrical Engineering, Universidad de Talca, Curicó, Chile

Correspondence
Leposava Ristić, School of Electrical Engineering, Bulevar kralja Aleksandra 73, Belgrade 11000, Serbia.
Email: leposava.ristic@etf.bg.ac.rs

Funding information
Ministry of Education, Science and Technological Development, Republic of Serbia, Grant/Award Number: 2022/200103; CLIMAT, Grant/Award Number: AMSUD210001; Fondecyt Regular, Grant/Award Number: 1220556

Abstract

This paper investigates space-vector-modulation (SVM) technique that uses only rotating space vectors to drive a direct matrix converter (DMC) with zero common-mode voltage (CMV). Two methods for controlling grid power factor have been proposed in the literature for such a drive. Until now, analysis has been limited to balanced grid conditions. However, total harmonic distortion (THD) of grid currents significantly increases under unbalanced conditions. Hence, the aims of this paper are: (1) derivation of DMC model consisting of general equations for output voltages and input currents, written in the complex form. (2) Analysis and comparison of two existing methods for grid power factor control under balanced grid conditions, by using the previously derived model. (3) Proposal of extended versions of both methods in order to improve converter's performance under unbalanced grid conditions. The proposed control strategy aims to achieve sinusoidal currents and maintain the same power factor on the grid side while completely compensating grid unbalance on the load side. (4) Determination of the maximum transfer ratio under balanced and unbalanced grid conditions. Experimental results with Hardware In the Loop (HIL) are provided to verify the theoretical analysis and effectiveness of the proposed control strategy.

1 | INTRODUCTION

Matrix converters (MC) are direct AC/AC power topologies without intermediate energy storage elements. Architectures based on MC provide a more-silicon solution with reduced needs for passive components, leading to high-performance and high-power-density electric drives. These requirements are essential for aircraft applications where size and weight are critical parameters [1]. Furthermore, it has been shown that MC are suitable for various modern industrial applications such as variable speed drives [2, 3], distributed power generation systems [4, 5], wind energy [6], and unified power flow controllers (UPFC) [7, 8].

In most grid-connected applications, control strategies applied to matrix converter aim to achieve sinusoidal and balanced output voltages with varying amplitude and frequency while drawing sinusoidal currents with controllable power factor angle from the grid. There are two main reasons why grid power factor angle should be controllable:

1. Reactive grid power control [9–19]. Under balanced grid conditions, reactive power is controlled by setting the grid power factor angle to a constant value once the steady state with established active and reactive power required by the consumer is reached. In order to meet the requirements for the unity grid power factor, separate control of the grid and load power factor is needed [9–11]. However, the potential use of MC in distributed power generation systems and other applications expands the requirements for reactive power control [12–19]. One can distinguish two general approaches to reactive grid power control [17]. According to the first approach, the grid-side reactive current is made from the reactive part of the load-side current [14, 15]. Modulation techniques adopting the second approach for controlling the grid-side reactive current incorporate the load-side active current [16]. Some more complex methods propose modulation techniques that combine both approaches to expand the range in which grid power factor can be controlled [17–19].

2. Grid current THD improvement under unbalanced grid conditions [11, 20–30]. Modulating the grid power factor angle dynamically around its constant value allows low-frequency harmonics to be significantly suppressed or even eliminated from the grid currents waveforms [20, 21]. Following the same idea, but applying different control strategies based on space-vector-modulation (SVM) modulation [22–24], mathematical construction of MC [25], notch filters [26], reference generation of reactive power [27, 28], feedback control [29], and model predictive control [30] has been proposed in the literature.

Conventional pulse-width modulation schemes [31] produce a high-frequency common-mode voltage (CMV) at the machine terminals, which causes bearing [32] and circulating currents [33] in electric drives and also increases requirements for common-mode noise filtering. By using Ventruini's first method [34], the matrix converter can be modulated using only the switching states that can eliminate the high-frequency CMV and generate rotating voltage vectors at the machine terminals. For conventional 3 × 3 MC-based drives, the SVM technique that uses only rotating vectors (RVs) has been investigated in many papers [35–40]. It has been shown that output reference voltages of desired amplitude and frequency can be generated using only rotating voltage vectors. However, voltage gain q in standard 3 × 3 MC topology is limited to 0.5, which is insufficient for most practical applications.

On the other hand, direct torque control using only RVs can achieve greater voltage gain $q = 0.833$, as shown in [41]. To increase voltage gain up to $q = 1.5$, topology presented in Figure 1 has been proposed in [42, 43], where two 3 × 3 MCs are applied, one at each side of an open-end-winding ac machine. Finally, grid power factor angle can also be controlled by using only RVs to control the reactive power [15, 16] and improve the THD of the grid current under unbalanced grid conditions [22]. However, analysis in [22] has been limited to the unity power factor, while the improvement of the grid current THD under unbalanced conditions has been verified only by simulation results, without experimental results and theoretical analysis.

This paper has four main aims, each one presented and analysed in a separate section:

1. The SVM technique that uses only RVs to drive an open-end-winding drive is analysed in Section 2. Furthermore, a new MCs model for such a drive consisting of general equations for output voltages and input currents, written in the complex form, is proposed and derived in this section.
2. Two methods for controlling reactive power [15, 16] are analysed and compared in Section 3 using the previously derived model.
3. Section 4 proposes new, extended versions of both methods to improve the converter's performance under unbalanced grid conditions. The proposed control strategy aims to achieve sinusoidal currents and maintain the same power factor on the grid side while completely compensating grid unbalance on the load side, establishing the paper's main contribution. Conventional methods presented in [27–30] require input current measurement, current or reactive power reference generation, and control in the closed loop, where the THD of the input current depends on the control loop's bandwidth. Higher harmonics in the input current can only be suppressed to a certain amount. On the other hand, with proposed control strategy, the influence of the grid unbalance on the load side of the matrix converter is eliminated in a feed-forward manner. As shown analytically and experimentally, the proposed method inherently achieves sinusoidal input currents under unbalanced conditions requiring only input voltage measurements, without closed-loop control. However, extracting the grid voltage's positive and negative sequence components results in a slightly more complex signal processing and modulation scheme.
4. The maximum voltage transfer ratio which can be reached under unbalanced grid conditions is determined in Section 5.

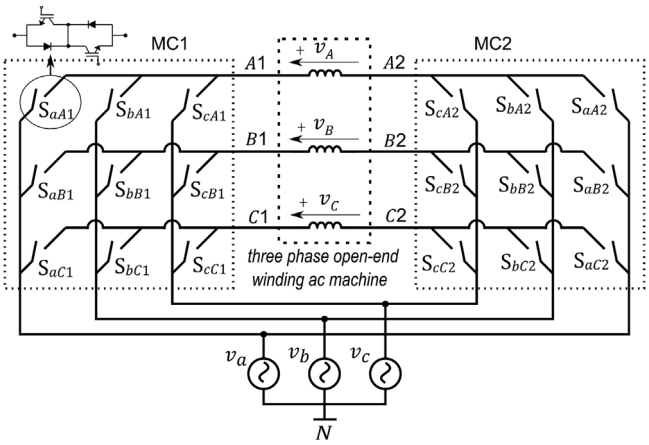

FIGURE 1 Open-end-winding drive based on DMC. DMC, direct matrix converter.

Finally, the HIL experimental results are provided in Section 6 to validate the theoretical analysis and proposed methods.

2 | NOVEL DIRECT MATRIX CONVERTER MODEL

A conventional 3 × 3 direct matrix converter (DMC) driving three-phase ac machine with a star-connected winding configuration can achieve a maximum voltage gain of $q = 0.5$, which is insufficient for most applications in drives. Besides, some input power factor control methods reduce voltage gain even further, as will be explained in Section 3. Furthermore, to compensate for the effect of unbalanced grid conditions on the load side of the matrix converter, the maximum gain is even further reduced, which is the subject of Section 5. The open-end winding-based drive shown in Figure 1 can achieve three times greater voltage gain up to $q = 1.5$ and therefore is a more suitable solution for most practical applications, regardless of twice as many active

semiconductor components. In this section, the SVM modulation technique for such an open-end-winding drive is discussed in detail.

For the open-end-winding drive presented in Figure 1, the CMV at the open-end-winding machine terminals (v_{cmv1}, v_{cmv2}) is defined by (1). The resultant CMV, defined as $v_{cmv,res} = (v_{cmv1} + v_{cmv2})/2$, causes bearing currents [32]. On the other hand, differential CMV across the open-end-winding machine defined as $v_{cmv,diff} = v_{cmv1} - v_{cmv2}$ causes circulating currents in open-end-winding drives [33].

$$v_{cmv1,2}(t) = \frac{v_{A1,2}(t) + v_{B1,2}(t) + v_{C1,2}(t)}{3} \tag{1}$$

For topology presented in Figure 1, 18 switching combinations can achieve zero CMV at the output terminals of the MC, eliminating bearing and circulating currents in that way. Nine of them result in counterclockwise (CCW) RV, while the remaining nine generate clockwise (CW) RV. Even though output voltage space vector can be synthesized using only CCW or CW rotating pairs of vectors, a combined modulation technique that uses both pairs of vectors has several significant benefits, as explained in the following sections.

2.1 | Modulation using CCW rotating vectors

Input and output three-phase voltages can be represented by instantaneous space vectors defined by (2) and (3). Factor 2/3 is used so that the magnitude of the voltage space vector is equal to the amplitude of the phase voltage.

$$\underline{V_g} = \frac{2}{3}\left(v_a(t)\,e^{i0} + v_b(t)\,e^{+i\frac{2\pi}{3}} + v_c(t)\,e^{-i\frac{2\pi}{3}}\right) \tag{2}$$

$$\underline{V_o} = \frac{2}{3}\left(v_{A1}(t)\,e^{i0} + v_{B1}(t)\,e^{+i\frac{2\pi}{3}} + v_{C1}(t)\,e^{-i\frac{2\pi}{3}}\right) - \frac{2}{3}\left(v_{A2}(t)\,e^{i0} + v_{B2}(t)\,e^{+i\frac{2\pi}{3}} + v_{C2}(t)\,e^{-i\frac{2\pi}{3}}\right) \tag{3}$$

Suppose that input phase voltages are connected to the output terminals of the matrix converter in the way that phase order remains the same. In that case, the output voltage space vector rotates in the same CCW direction as the input voltage vector. By using Equations (2), (3), and (4), nine switching states ($i = 1:9$) that generate CCW RV $\underline{V_{occwi}}$ on the output terminals can be presented by discrete values of complex modulation index $\underline{m_{ccwi}}$ listed in Table 1. Six of them guide to non-zero CCW RV with $\sqrt{3}$ times greater amplitude and different phase shifts with respect to grid space vector. The remaining three are zero voltage vectors, obtained by cancelling two CCW RV with the same amplitudes and phases on each side of the three-phase open-end-winding load. So, compared to the modulation index used to represent only the amplitude gain, the complex modulation index also carries information about the phase shift of the output voltage space vector with respect to the grid space vector. The corresponding vectors are plotted on the complex plane, as shown in Figure 2a. For all switching states listed in Table 1, CMVs at the open-end-winding terminals $v_{cmv1,2}$ are equal to zero according to (1), assuming that $v_a + v_b + v_c = 0$.

TABLE 1 Switching states generating CCW vectors

$\underline{m_{ccwi}}$	A1	B1	C1	A2	B2	C2	Equation (4)
$\underline{m_{ccw1}}$	a	b	c	b	c	a	$\sqrt{3}e^{+i\frac{\pi}{6}}$
$\underline{m_{ccw2}}$	c	a	b	b	c	a	$\sqrt{3}e^{+i\frac{\pi}{2}}$
$\underline{m_{ccw3}}$	c	a	b	a	b	c	$\sqrt{3}e^{+i\frac{5\pi}{6}}$
$\underline{m_{ccw4}}$	b	c	a	a	b	c	$\sqrt{3}e^{-i\frac{5\pi}{6}}$
$\underline{m_{ccw5}}$	b	c	a	c	a	b	$\sqrt{3}e^{-i\frac{\pi}{2}}$
$\underline{m_{ccw6}}$	a	b	c	c	a	b	$\sqrt{3}e^{-i\frac{\pi}{6}}$
$\underline{m_{ccw7}}$	b	c	a	b	c	a	0
$\underline{m_{ccw8}}$	c	a	b	c	a	b	0
$\underline{m_{ccw9}}$	a	b	c	a	b	c	0

$$\underline{m_{ccwi}} = \frac{\underline{V_{occwi}}}{\underline{V_g}} \tag{4}$$

Let us define the desired complex modulation index as $\underline{m_{ccw}^{ref}} = \frac{3}{2}\,m_{ccw}^{ref}\,e^{i\theta_{ccw}^{ref}}$ where m_{ccw}^{ref} is the reference modulation index and θ_{ccw}^{ref} is the reference angle. It can be synthesized during one switching period Ts by applying two adjacent active switching vectors ($\underline{m_x}$, $\underline{m_y}$) and one zero vector ($\underline{m_0}$) for a certain fraction of switching period Ts (d_{ccw1}, d_{ccw2}, d_{ccw0}), as described in (5). Hence, $\underline{m_{ccw}}$ represent the average value of complex modulation index over one switching period.

$$\underline{m_{ccw}} = d_{ccw1}\,\underline{m_x} + d_{ccw2}\,\underline{m_y} + d_{ccw0}\,\underline{m_0} \tag{5}$$

The sector in which the reference space vector is located is determined based on the reference value of the angle θ_{ccw}^{ref}. Afterwards, Table 2 reveals which vectors are active depending on the ordinal number of the sector N in which the reference vector is located. Finally, the duty cycles of the corresponding vectors are calculated using Equations (6) to (8). Angle Φ_v is defined as the limiting value of the angle range in a corresponding sector. From Figure 2a, one can observe that the maximum value of converter voltage gain q for SVM operating in the linear range is $q_{max} = 1.5$. By varying modulation index m_{ccw}^{ref} from 0 to 1, converter voltage gain changes from 0 to 1.5.

$$d_{ccw1} = m_{ccw}^{ref}\,\sin\left(\Phi_v - \theta_{ccw}^{ref}\right) \tag{6}$$

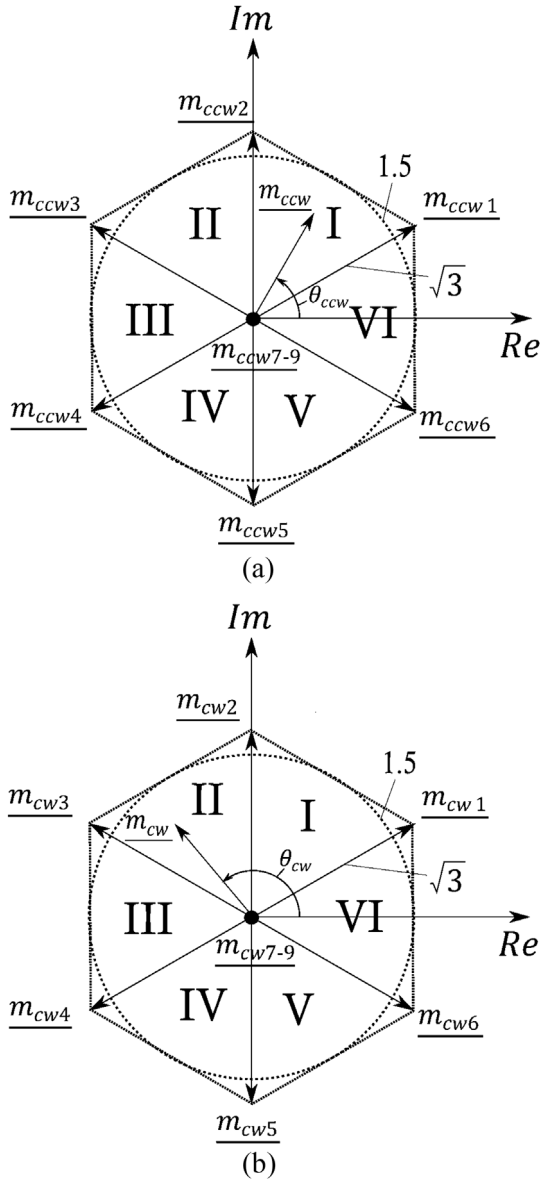

FIGURE 2 Space-vector modulation using (a) CCW rotating vectors, **(b)** CW rotating vectors. CCW, counterclockwise; CW, clockwise.

TABLE 2 Look-up table of active vectors

Sector	$\underline{m_x}$	$\underline{m_y}$	$\underline{m_0}$	Φ_v
I	$\underline{m_{ccw1}}$	$\underline{m_{ccw2}}$	$\underline{m_{ccw7}}$	$\frac{\pi}{2}$
II	$\underline{m_{ccw2}}$	$\underline{m_{ccw3}}$	$\underline{m_{ccw8}}$	$\frac{5\pi}{6}$
III	$\underline{m_{ccw3}}$	$\underline{m_{ccw4}}$	$\underline{m_{ccw9}}$	$-\frac{5\pi}{6}$
IV	$\underline{m_{ccw4}}$	$\underline{m_{ccw5}}$	$\underline{m_{ccw7}}$	$-\frac{\pi}{2}$
V	$\underline{m_{ccw5}}$	$\underline{m_{ccw6}}$	$\underline{m_{ccw8}}$	$-\frac{\pi}{6}$
VI	$\underline{m_{ccw6}}$	$\underline{m_{ccw1}}$	$\underline{m_{ccw9}}$	$\frac{\pi}{6}$

TABLE 3 Switching states generating CW vectors

$\underline{m_{cwi}}$	*A1*	*B1*	*C1*	*A2*	*B2*	*C2*	Equation (11)
$\underline{m_{cw1}}$	*a*	*c*	*b*	*c*	*b*	*a*	$\sqrt{3}e^{+i\frac{\pi}{6}}$
$\underline{m_{cw2}}$	*b*	*a*	*c*	*c*	*b*	*a*	$\sqrt{3}e^{+i\frac{\pi}{2}}$
$\underline{m_{cw3}}$	*b*	*a*	*c*	*a*	*c*	*b*	$\sqrt{3}e^{+i\frac{5\pi}{6}}$
$\underline{m_{cw4}}$	*c*	*b*	*a*	*a*	*c*	*b*	$\sqrt{3}e^{-i\frac{5\pi}{6}}$
$\underline{m_{cw5}}$	*c*	*b*	*a*	*b*	*a*	*c*	$\sqrt{3}e^{-i\frac{\pi}{2}}$
$\underline{m_{cw6}}$	*a*	*c*	*b*	*b*	*a*	*c*	$\sqrt{3}e^{-i\frac{\pi}{6}}$
$\underline{m_{cw7}}$	*c*	*b*	*a*	*c*	*b*	*a*	0
$\underline{m_{cw8}}$	*b*	*a*	*c*	*b*	*a*	*c*	0
$\underline{m_{cw9}}$	*a*	*c*	*b*	*a*	*c*	*b*	0

$$d_{ccw2} = m_{ccw}^{ref} \sin\left(\frac{\pi}{3} - \Phi_v + \theta_{ccw}^{ref}\right) \tag{7}$$

$$d_{ccw0} = 1 - d_{ccw1} - d_{ccw2} \tag{8}$$

The average voltage space vector at the output terminals can be written in the following form:

$$\underline{V_{occw}} = \underline{m_{ccw}}\ \underline{V_g} \tag{9}$$

On the input side of the MC, the average current space vector given by (10) is derived from the power equilibrium equation, where the output voltage vector $\underline{V_{occw}}$ is substituted with expression (9).

$$\underline{V_g}\ \underline{I_{gccw}^*} = \underline{V_{occw}}\ \underline{I_o^*} \rightarrow \underline{I_{gccw}} = \underline{m_{ccw}^*}\ \underline{I_o} \tag{10}$$

Equation (10) reveals that input current is equal to the product of conjugate (designated with *) of complex modulation index and output current vector $\underline{I_o}$.

2.2 | Modulation using CW rotating vectors

By changing the order of input phases when connecting them to the output terminals of the matrix converter, the output voltage space vector starts rotating in the opposite (clockwise) direction from the input vector. Hence, the conjugate value of the grid voltage vector is used to represent the complex modulation index. As stated in the previous case, discrete values of complex modulation indexes referring to nine switching states generating CW RV are derived by using Equations (2), (3), (11) and presented in Table 3 and Figure 2b. It should be noted that these switching states also result in zero CMVs at output terminals as ones generating CCW RV (Table 1), except that phases *b* and *c*

have swapped positions.

$$\underline{m_{cwi}} = \frac{\underline{V_{ocwi}}}{\underline{V_g^*}} \tag{11}$$

Discrete values of complex modulation index $\underline{m_{cwi}}$ are used to synthesize the average reference value $\underline{m_{cw}}$ in the same manner as previously explained when modulation using CCW RV was investigated. The average voltage space vector at the output terminals is defined by (12).

$$\underline{V_{ocw}} = \underline{m_{cw}}\ \underline{V_g^*} \tag{12}$$

As before, substituting (12) into power equilibrium Equation (13), the expression of input current vector $\underline{I_{gcw}}$ can be derived. On the left side of the power equilibrium equation, conjugate values of grid voltage and current vectors are used because phases *b* and *c* have swapped positions.

$$\underline{V_g^*}\ \underline{I_g} = \underline{V_{ocw}}\ \underline{I_o^*} \rightarrow \underline{I_{gcw}} = \underline{m_{cw}}\ \underline{I_o^*} \tag{13}$$

2.3 | Combined modulation technique

The basic idea of the combined modulation technique is to modulate the output voltage vector by using both CCW and CW RV. During the first part of the switching period, two active and one zero CCW vectors are used to synthesize the CCW component $\underline{V_{occw}}$ of the output voltage space vector. The same principle is used only with CW RV during the second part of the switching period when the CW component $\underline{V_{ocw}}$ is generated. The average value of the output voltage space vector over one switching period is defined by (14) and equal to the vector sum of two components. Similarly, on the input side of the MC, the average value of the current vector is defined by (15). Equations (14) and (15) represent the model of DMC written in the complex form, which provides a deeper insight into matrix converter performance under different kinds of input or output disturbances.

$$\underline{V_o} = \overbrace{\underline{m_{ccw}}\ \underline{V_g}}^{\underline{V_{occw}}} + \overbrace{\underline{m_{cw}}\ \underline{V_g^*}}^{\underline{V_{ocw}}} \tag{14}$$

$$\underline{I_g} = \overbrace{\underline{m_{ccw}^*} \underline{I_o}}^{\underline{I_{gccw}}} + \overbrace{\underline{m_{cw}} \underline{I_o^*}}^{\underline{I_{gcw}}} \tag{15}$$

An important feature of the combined modulation technique is that both MCs participate equally in generating the output voltage's CCW and CW components. Therefore, the proposed modulation technique is expected to achieve equal power distribution among two MCs. Suppose that the reference CCW vector is in a Sector I. According to Table 2 $\underline{m_{ccw1}}$, $\underline{m_{ccw2}}$ and $\underline{m_{ccw7}}$ are active and used for modulating the reference vector. Table 1 shows that those switching states result in modulating the reference vector only by switching MC1 ($A1B1C1 = abc \rightarrow cab \rightarrow bca$) while the switching configuration of MC2 is not changing during this time ($A2B2C2 = bca$). In the next sector, MC2 modulates the reference vector, while the switching configuration of MC1 remains the same. During the period required for the reference vector to turn a full circle, MC1 and MC2 participate in the modulation of the reference vector equally. The same logic refers to the modulation of the CW reference vector.

However, due to the increased number of vectors used to generate a reference output voltage, switching losses of matrix converter are expected to increase. The sum of all duty cycles of the six corresponding vectors that are used (d_{ccw0}, d_{ccw1}, d_{ccw2}, d_{cw0}, d_{cw1}, d_{cw2}) during the one switching period must be equal to 1. Despite increased switching losses, it is of interest to modulate the output voltage vector using both CCW and CW rotating pairs of vectors. In that way, the input power factor angle can be controllable, which is essential for several reasons, as explained in the following sections.

3 | TWO METHODS FOR CONTROLLING GRID POWER FACTOR

Output voltage space vector can be generated only by using CCW or CW rotating voltage vectors. However, the input phase angle is equal or opposite to the output phase angle, depending on whether the direction of the resultant output voltage space vector coincides with the direction of RV that are generating it [42]. Hence, it is impossible to control the input power factor or modulate the input phase angle to improve the power quality under unbalanced conditions. On the other hand, a combined modulation technique that uses both CCW and CW RV can achieve both aims at the cost of increased switching losses. This section investigates two grid power factor control methods based on combined modulation under balanced grid conditions using the previously derived model of a DMC. Grid space vector under balanced conditions is given by (16), where V^+ and ω_g stand for amplitude and the angular frequency of the grid phase voltages.

$$\underline{V_g} = V^+\ e^{j\omega_g t} \tag{16}$$

The input power factor equals unity if CCW and CW output voltage components are equal in amplitude and phase [14]. By changing the phase [16] (Method I) or amplitude [15] (Method II) in the appropriate ratio, the input power factor can be controlled. Two methods differ in the range in which the grid power factor angle can be controlled, as well as output voltage capability.

3.1 | Method I—Combined modulation with phase control

This method controls phases of CCW and CW output voltage components while keeping them equal in amplitude (Figure 3a).

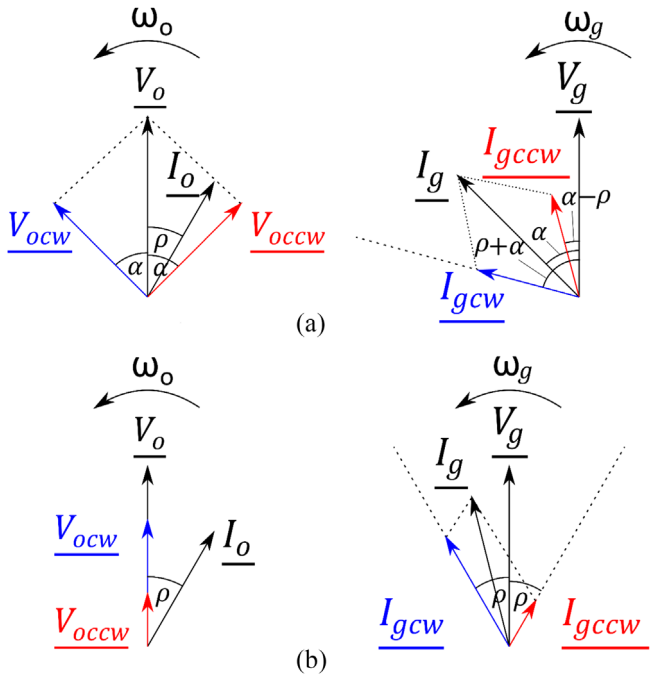

FIGURE 3 Control of grid power factor: (a) method I, (b) method II

CCW and CW rotating pairs of vectors are applied each for precisely one half of the switching period $\frac{T_s}{2}$ in such a way that the resultant CCW and CW output voltage components are equal in amplitude and shifted in phase by angle 2α. This method can also be presented by the complex modulation indexes (17) and (18).

$$\underline{m_{ccw}} = \frac{3}{4}\, m e^{j(\omega_o-\omega_g)t}\, e^{-i\alpha} \tag{17}$$

$$\underline{m_{cw}} = \frac{3}{4}\, m e^{j(\omega_o+\omega_g)t}\, e^{j\alpha} \tag{18}$$

Modulation index m is used for controlling the amplitude and ω_o refers to the angular frequency of the output voltage. Substituting (16), (17), and (18) into (14) gives an expression for the output voltage space vector (19).

$$\underline{V_o} = \overbrace{\frac{3}{4} m V^+ e^{j(\omega_o t-\alpha)}}^{\underline{V_{occw}}} + \overbrace{\frac{3}{4} m V^+ e^{j(\omega_o t+\alpha)}}^{\underline{V_{ocw}}}$$

$$= \frac{3}{2} V^+ m \cos\alpha e^{j\omega_o t} \tag{19}$$

Assuming that the load is linear, the output current can be written in the following form:

$$\underline{I_o} = I_o\, e^{j(\omega_o t-\rho)} \tag{20}$$

where amplitude I_o and output power angle ρ depend on load characteristics. By substituting (17), (18), and (20) into (15), the expression for the grid current vector (21) can be derived.

$$\underline{I_g} = \overbrace{\frac{3}{4} m I_o e^{j(\omega_g t+\alpha-\rho)}}^{\underline{I_{gccw}}} + \overbrace{\frac{3}{4} m I_o e^{j(\omega_g t+\alpha+\rho)}}^{\underline{I_{gcw}}}$$

$$= \frac{3}{2} I_o m \cos\rho e^{j(\omega_g t+\alpha)} \tag{21}$$

Equation (21) reveals that the grid power factor angle Φ is equal to α and independent of the output power factor angle ρ. Hence, it can be controlled in any range $-\frac{\pi}{2} \le \Phi \le \frac{\pi}{2}$, but the output voltage decreases with the power factor $\cos\Phi$, as shown in (19). Finally, using expressions for grid voltage (16) and current (21) space vectors, input power under balanced input conditions can be written in the following form:

$$\underline{S_g} = \frac{3}{2}\, \underline{V_g}\, \underline{I_g^*}$$

$$= \overbrace{\frac{9}{4} V^+ I_o m \cos\rho\cos\alpha}^{P_g} - i \overbrace{\frac{9}{4} V^+ I_o m \cos\rho \sin\alpha}^{Q_g} \tag{22}$$

From (22), it can be observed that reactive output power does not influence the reactive input power. Hence, this method is advantageous in applications where reactive output power does not meet the restrictions for reactive power on the grid side. However, the converter's output voltage and active power capability decrease with the reactive grid power.

3.2 | Method II—Combined modulation with amplitude control

Contrary to method I, method II controls the CCW and CW output voltage component's amplitudes while keeping them equal in phase (Figure 3b). During the first part of the switching period ($0 \le t \le kT_s$), the CCW output voltage component ($\underline{V_{occw}}$) is synthesized using CCW RV, and its amplitude is proportional to k. During the second part of the switching period ($kT_s \le t \le T_s$), the CW output voltage component ($\underline{V_{ocw}}$) is synthesized using CW RV, and its amplitude is proportional to $(1-k)$. This concept is presented by the complex modulation indexes (23) and (24).

$$\underline{m_{ccw}} = \frac{3}{2}\, m e^{j(\omega_o-\omega_g)t}\, k \tag{23}$$

$$\underline{m_{cw}} = \frac{3}{2}\, m e^{j(\omega_o+\omega_g)t}\, (1-k) \tag{24}$$

By substituting (23), (24), and (16) into (14), we get the expression for the voltage vector (25) on the output terminals.

$$\underline{V_o} = \overbrace{\frac{3}{2} m V^+ e^{j\omega_o t}\, k}^{\underline{V_{occw}}} + \overbrace{\frac{3}{2} m V^+ e^{j\omega_o t}\, (1-k)}^{\underline{V_{ocw}}}$$

$$= \frac{3}{2} V^+ m e^{j\omega_o t} \tag{25}$$

The grid current vector expression (26) is derived by substituting (23), (24), and (20) into (15).

$$\begin{aligned}\underline{I_g} &= \overbrace{\frac{3}{2}mI_o e^{j(\omega_g t-\rho)}}^{\underline{I_{gccw}}}k + \overbrace{\frac{3}{2}mI_o e^{j(\omega_g t+\rho)}}^{\underline{I_{gcw}}}(1-k)\\ &= \frac{3}{2}mI_o e^{j\omega_g t}\left(ke^{-i\rho} + (1-k)\,e^{i\rho}\right)\end{aligned} \tag{26}$$

From (26), it can be observed that the input power factor angle Φ can be controlled in the range of $-\rho \le \Phi \le \rho$ by varying coefficient k in the range $0 \le k \le 1$ without reducing output voltage capability, as shown in (25). Equation (27) reveals that reactive grid power is controlled by coefficient k in the range limited by the positive and negative value of the reactive output power. If the reactive output power is sufficient to meet the grid needs, this method is preferred due to no reduction in the converter's output voltage or active power capability.

$$\underline{S_g} = \overbrace{\frac{9}{4}V^+ I_o m\cos\rho}^{P_g} - i\overbrace{\frac{9}{4}V^+ I_o m\,(1-2k)\sin\rho}^{Q_g} \tag{27}$$

The preferred method depends on the operating point of the converter. For input power factor angle in the range of $|\Phi| \le \rho$, method II (amplitude control) is preferable because it, unlike method I, does not require reduction of the output voltage. On the other hand, only method I (phase control) can control the input power factor in the extended range of $\rho < |\Phi| \le \frac{\pi}{2}$. The simple control algorithm, which will use the optimal method depending on the range in which the input power factor is controlled, should result in better overall performance. This way, the input power factor is controlled by modulating only the amplitude or phase of the CCW and CW components in a particular operating region. On the other hand, controlling both phase and amplitude in the whole range expands the power factor control to its absolute maximum values limited only by the linear operation of SVM. Even though such a control strategy results in the best overall performance in the whole power factor range, it becomes much more complex and therefore remains for future work.

4 | IMPROVEMENT OF TWO POWER FACTOR CONTROL METHODS

This section analyzes methods from Section 3 under unbalanced grid conditions. Due to an increase in THD of both input and output currents, methods need to be improved. Hence, extended versions of both methods are proposed to improve the converter's performance under unbalanced grid conditions.

4.1 | Analysis under unbalanced conditions

The grid space vector defined by (28) has both positive $\underline{V_g^+}$ and negative $\underline{V_g^-}$ sequence components under unbalanced conditions. V^- and θ^- refer to the amplitude and initial phase angle of the negative sequence component. Factor u is defined by (29) and represents grid voltage imbalance degree.

$$\underline{V_g} = \overbrace{V^+ e^{j\omega_g t}}^{\underline{V_g^+}} + \overbrace{V^- e^{j(-\omega_g t-\theta^-)}}^{\underline{V_g^-}} \tag{28}$$

$$u = \frac{V^-}{V^+} \tag{29}$$

The following analysis aims to show how the negative sequence component of the grid voltage affects the THD of the input and output currents. The two methods at the unity power factor result in identical expressions for the complex index modulation. By inserting the value $\alpha = 0$ into Equations (17) and (18) or $k = 0.5$ into Equations (23) and (24), the corresponding expressions given by (30) and (31) are obtained.

$$\underline{m_{ccw}} = \frac{3}{4}\,me^{j(\omega_o-\omega_g)t} \tag{30}$$

$$\underline{m_{cw}} = \frac{3}{4}\,me^{j(\omega_o+\omega_g)t} \tag{31}$$

By substituting (30), (31), and (28) into (14), expression (32) for the output voltage vector under unbalanced grid conditions is obtained.

$$\begin{aligned}\underline{V_o} = &\frac{3}{2}\,mV^+ e^{j\omega_o t} + \frac{3}{4}mV^- e^{j(\omega_o t-2\omega_g t-\theta^-)}\\ &+ \frac{3}{4}mV^- e^{j(\omega_o t+2\omega_g t+\theta^-)}\end{aligned} \tag{32}$$

From (32), it can be observed that positive sequence components of grid voltage will result in the wanted component of the output voltage at the desired frequency ω_o while the negative sequence component will generate two unwanted components at $\omega_o - 2\omega_s$ and $\omega_o + 2\omega_s$ angular frequencies. The same frequency components appear in the output current if the load is linear, while each specific component's amplitude (I_o, I_{o1}, I_{o2}) and phase shift (ρ, ρ_1, ρ_2) depend on the load characteristics. Therefore, the output current vector can be written in the following form:

$$\begin{aligned}\underline{I_o} = &I_o\, e^{j(\omega_o t-\rho)} + I_{o1}\, e^{j(\omega_o t-2\omega_g t-\theta^--\rho_1)}\\ &+ I_{o2} e^{j(\omega_o t+2\omega_g t+\theta^--\rho_2)}\end{aligned} \tag{33}$$

By substituting (30), (31), and (33) into (15), an expression for the input current given by (34) is derived.

$$\begin{aligned}\underline{I_g} = &\frac{3}{2}\,mI_o\cos\rho e^{j\omega_g t}\\ &+ \frac{3}{4}me^{-i(\omega_g t+\theta^-)}\left(I_{o1}e^{-i\rho_1} + I_{o2}e^{i\rho_2}\right)\\ &+ \frac{3}{4}me^{j(3\omega_g t+\theta^-)}\left(I_{o1}e^{i\rho_1} + I_{o2}e^{-i\rho_2}\right)\end{aligned} \tag{34}$$

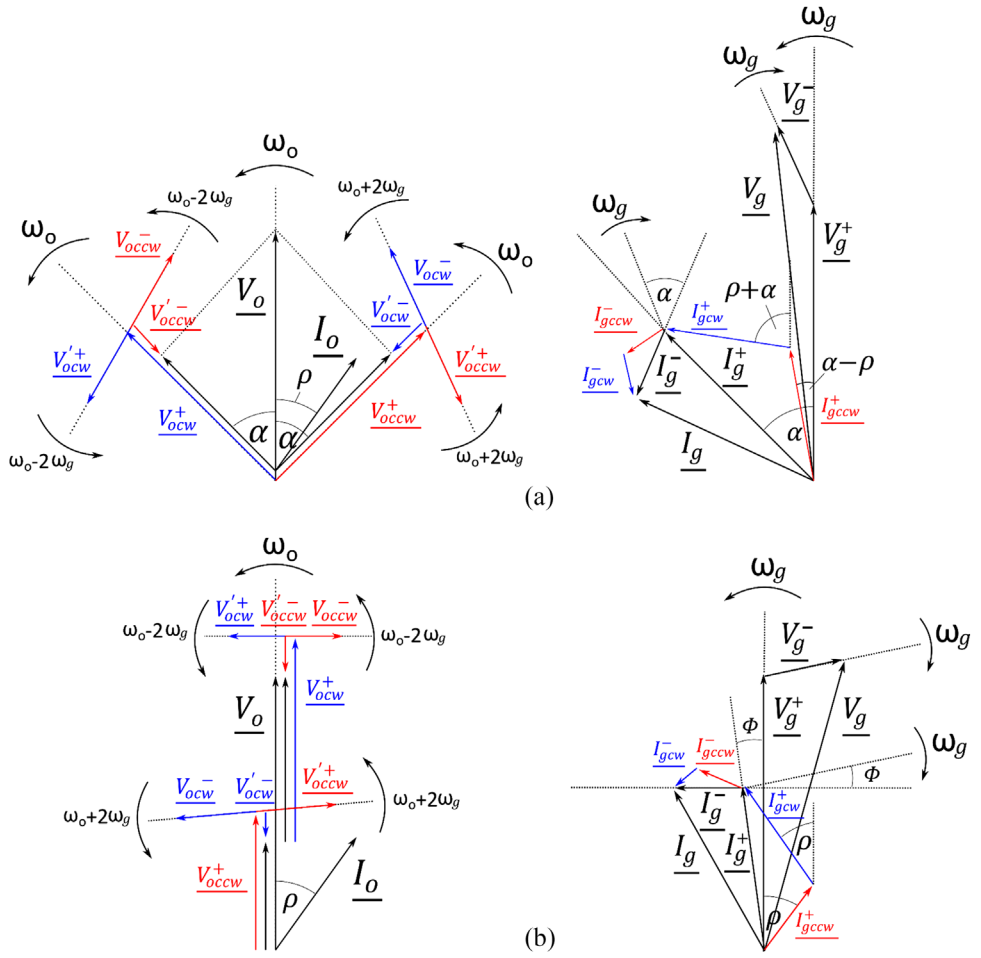

FIGURE 4 Improvement of two methods operating under unbalanced grid conditions. Extended version of (a) method I, (b) method II

Equation (34) reveals that unwanted components in the output current cause negative sequence component and undesired third harmonic in the input current waveform. Due to the unwanted components in the input and output currents waveforms, there is a necessity to expand the existing methods for power factor control.

According to [20], MC tied to an unbalanced grid should adopt a control strategy that aims to completely compensate the input unbalance on the output side of the converter while achieving sinusoidal but unbalanced input currents and maintaining control of grid power factor. Hence, extended versions of the two methods are presented in this section to improve the power quality of DMC-based drive operating under unbalanced grid conditions. The same concept, presented in Figure 4, is used for both power factor control methods. Namely, unwanted component ($\underline{V_{occw}^{-}}$) of the output space vector generated during the first part of the switching period when CCW vectors are active can be eliminated during the second part of the switching period by using CW RV to generate one additional component ($\underline{V_{ocw}^{\prime +}}$) equal in amplitude and frequency, but opposite in phase to the unwanted one. In the same manner, unwanted component ($\underline{V_{ocw}^{-}}$) generated during the second part of the switching period when CW RV are active, can be compensated using CCW RV to generate additional component ($\underline{V_{occw}^{\prime +}}$) during the first part of the switching period.

4.2 | Improvement of method I—Phase control

The extended version of method I is represented by complex modulation indexes (35) and (36). In each expression, one additional negative term is added, to cancel out the unwanted voltage components resulting from imbalanced grid voltage. The modulation index m must be extended to m' following Equation (37) to maintain the same output voltage amplitude, by taking into account the grid voltage imbalance factor u, defined in (29).

$$\underline{m_{ccw}} = \frac{3}{4} m' e^{j(\omega_o t - \omega_g t - \alpha)} - \frac{3}{4} m' u e^{j(\omega_o t + \omega_g t + \theta^{-} + \alpha)} \tag{35}$$

$$\underline{m_{cw}} = \frac{3}{4} m' e^{j(\omega_o t + \omega_g t + \alpha)} - \frac{3}{4} m' u e^{j(\omega_o t - \omega_g t - \theta^{-} - \alpha)} \tag{36}$$

$$m' = m \frac{1}{1 - u^2} \tag{37}$$

By substituting Equations (28), (35), (36) into (14), the output voltage vector is derived and presented in (38).

$$\begin{aligned}\underline{V_o} &= \underline{m_{ccw}}\overbrace{\left(\underline{V_g^+}+\underline{V_g^-}\right)}^{\underline{V_g}}+\underline{m_{cw}}\overbrace{\left(\underline{V_g^{+*}}+\underline{V_g^{-*}}\right)}^{\underline{V_g^*}}\\ &= \overbrace{\frac{3}{4}m' V^+ e^{j(\omega_o t-\alpha)}}^{\underline{V_{occw}^+}}+\overbrace{\frac{3}{4}m' V^- e^{j(\omega_o t-2\omega_g t-\alpha-\theta^-)}}^{\underline{V_{occw}^-}}\\ &\quad -\overbrace{\frac{3}{4}m' V^- e^{j(\omega_o t+2\omega_g t+\alpha+\theta^-)}}^{\underline{V_{occw}'^+}}-\overbrace{\frac{3}{4}m' uV^- e^{j(\omega_o t+\alpha)}}^{\underline{V_{occw}'^-}}\\ &\quad +\overbrace{\frac{3}{4}m' V^+ e^{j(\omega_o t+\alpha)}}^{\underline{V_{ocw}^+}}+\overbrace{\frac{3}{4}m' V^- e^{j(\omega_o t+2\omega_g t+\alpha+\theta^-)}}^{\underline{V_{ocw}^-}}\\ &\quad -\overbrace{\frac{3}{4}m' V^- e^{j(\omega_o t-2\omega_g t-\alpha-\theta^-)}}^{\underline{V_{ocw}'^+}}-\overbrace{\frac{3}{4}m' uV^- e^{j(\omega_o t-\alpha)}}^{\underline{V_{ocw}'^-}}=\\ &= \overbrace{\frac{3}{2}V^+ m' \cos\alpha e^{j\omega_o t}}^{\underline{V_{occw}^+}+\underline{V_{ocw}^+}}-\overbrace{\frac{3}{2}m' uV^- \cos\alpha e^{j\omega_o t}}^{\underline{V_{occw}'^-}+\underline{V_{ocw}'^-}}\end{aligned} \tag{38}$$

Following Equation (29), uV^- can be replaced with u^2V^+. By substituting m' with expression (37) and uV^- with u^2V^+, the final expression for the output voltage vector is derived and presented in (39).

$$\underline{V_o} = \frac{3}{2}\ V^+ m' \cos\alpha\left(1-u^2\right)\ e^{j\omega_o t} = \frac{3}{2}\ V^+ m \cos\alpha e^{j\omega_o t} \tag{39}$$

From (39), it can be observed that output voltage remains unchanged in the presence of unbalanced input conditions. Hence, the expression of the output current space vector remains the same as in (20). Combining (35), (36), (20), and (15), an expression for the input current vector (40) can be derived.

$$\begin{aligned}\underline{I_g} &= \underline{m_{ccw}^*}\ \underline{I_o}+\underline{m_{cw}}\ \underline{I_o^*}\\ &= \overbrace{\frac{3}{4}m' I_o e^{j(\omega_g t+\alpha-\rho)}}^{\underline{I_{gccw}^+}}-\overbrace{\frac{3}{4}m' I_o u e^{-i(\omega_g t+\theta^-+\alpha+\rho)}}^{\underline{I_{gccw}^-}}\\ &\quad +\overbrace{\frac{3}{4}m' I_o e^{j(\omega_g t+\alpha+\rho)}}^{\underline{I_{gcw}^+}}-\overbrace{\frac{3}{4}m' I_o u e^{-i(\omega_g t+\theta^-+\alpha-\rho)}}^{\underline{I_{gcw}^-}}\\ &\quad \underbrace{\frac{3}{2}m' \cos\rho I_o e^{j(\omega_g t+\alpha)}}_{\underline{I_g^+}}-\underbrace{\frac{3}{2}m' \cos\rho I_o u e^{-i(\omega_g t+\theta^-+\alpha)}}_{\underline{I_g^-}}\end{aligned} \tag{40}$$

From (40), it can be observed that both positive and negative sequence components at fundamental frequency are present. Still, there are no unwanted low-frequency harmonics, which means that the proposed control strategy is inherently capable of achieving sinusoidal input currents under unbalanced conditions. Finally, by using expressions for grid current (40) and voltage (28) vector, an expression for grid complex power (41) is obtained.

$$\begin{aligned}\underline{S_g} &= \frac{3}{2}\ \underline{V_g}\ \underline{I_g^*} = \overbrace{\frac{9}{4}V^+ I_o m \cos\rho\cos\alpha}^{P_g}\\ &\quad -i\overbrace{\frac{9}{4}V^+ I_o m \cos\rho\underbrace{\frac{1+u^2}{1-u^2}}_{\gamma}\sin\alpha}^{Q_g}\\ &\quad -i\overbrace{\frac{9}{2}V^- I_o m' \cos\rho\sin\left(2\omega_g t+\theta^-+\alpha\right)}^{q_{osc}}\end{aligned} \tag{41}$$

Compared to balanced grid conditions, the dc component of reactive power is slightly higher by factor γ, and the oscillating component occurs at twice the grid frequency. Instantaneous active power is equal to its dc component and remains unchanged compared to balanced grid conditions, which is expected considering the unchanged output characteristics of the converter.

4.3 | Improvement of method II—Amplitude control

Following the same idea, method II is extended by adding one additional term in expressions (42) and (43), representing modified complex modulation indexes.

$$\underline{m_{ccw}} = \frac{3}{2}\ m' e^{j(\omega_o-\omega_g)t}k-\frac{3}{2}m' ue^{j(\omega_o t+\omega_g t+\theta^-)}(1-k) \tag{42}$$

$$\underline{m_{cw}} = \frac{3}{2}\ m' e^{j(\omega_o+\omega_g)t}(1-k)-\frac{3}{2}m' ue^{j(\omega_o t-\omega_g t-\theta^-)}k \tag{43}$$

The voltage space vector at the output terminals is given by (44) and derived by substituting Equations (42), (43), and (28) into (14). The proposed method compensates the input unbalance at the converter's output terminals.

$$\begin{aligned}\underline{V_o} &= \overbrace{\frac{3}{2}m' V^+ e^{j\omega_o t}k}^{\underline{V_{occw}^+}}+\overbrace{\frac{3}{2}m' V^- e^{j(\omega_o t-2\omega_g t-\theta^-)}k}^{\underline{V_{occw}^-}}\\ &\quad -\overbrace{\frac{3}{2}m' V^- e^{j(\omega_o t+2\omega_g t+\theta^-)}(1-k)}^{\underline{V_{occw}'^+}}-\overbrace{\frac{3}{2}m' uV^- e^{j\omega_o t}(1-k)}^{\underline{V_{occw}'^-}}\end{aligned}$$

$$+\overbrace{\frac{3}{2}m'V^{+}e^{j\omega_o t}}^{\underline{V_{ocw}^{+}}}(1-k)+\overbrace{\frac{3}{2}m'V^{-}e^{j(\omega_o t+2\omega_g t+\theta^{-})}}^{\underline{V_{ocw}^{-}}}(1-k)$$

$$-\overbrace{\frac{3}{2}m'V^{-}e^{j(\omega_o t-2\omega_g t-\theta^{-})}}^{\underline{V_{ocw}^{\prime +}}}k-\overbrace{\frac{3}{2}m'uV^{-}e^{j\omega_o t}}^{\underline{V_{ocw}^{\prime -}}}k$$

$$=\frac{3}{2}V^{+}me^{j\omega_o t} \tag{44}$$

The grid current vector is presented in (45) and obtained by substituting Equations (42), (43), and (20) into (15). As with method I, the third harmonic is eliminated from the input currents waveforms.

$$\underline{I_g}=\overbrace{\frac{3}{2}m'I_o e^{j(\omega_g t-\rho)}}^{\underline{I_{gccw}^{+}}}k-\overbrace{\frac{3}{2}m'uI_o e^{-j(\omega_g t+\theta^{-}+\rho)}}^{\underline{I_{gccw}^{-}}}(1-k)$$

$$+\overbrace{\frac{3}{2}m'I_o e^{j(\omega_g t+\rho)}}^{\underline{I_{gcw}^{+}}}(1-k)-\overbrace{\frac{3}{2}m'uI_o e^{-j(\omega_g t+\theta^{-}-\rho)}}^{\underline{I_{gcw}^{-}}}k \tag{45}$$

$$=\overbrace{\frac{3}{2}m'I_o e^{j\omega_g t}\left(ke^{-j\rho}+(1-k)e^{j\rho}\right)}^{\underline{I_g^{+}}}$$

$$-\overbrace{\frac{3}{2}m'uI_o e^{-j(\omega_g t+\theta^{-})}\left(ke^{j\rho}+(1-k)e^{-j\rho}\right)}^{\underline{I_g^{-}}}$$

Grid power expression is given by (46). The same conclusions drawn in the analysis of the method I can be applied here. It should be noted that factor γ, which slightly increases the average value of grid reactive power, can be compensated by adapting coefficient k (or α for method I).

$$\underline{S_g}=\overbrace{\frac{9}{4}V^{+}I_o m\cos\rho}^{P_g}-i\overbrace{\frac{9}{4}V^{+}I_o m(1-2k)\underbrace{\frac{1+u^2}{1-u^2}}_{\gamma}\sin\rho}^{Q_g}$$

$$-i\overbrace{\frac{9}{2}V^{-}I_o m'k\sin\left(2\omega_g t+\theta^{-}-\rho\right)}^{q_{osc1}} \tag{46}$$

$$-i\overbrace{\frac{9}{2}V^{-}I_o m'(1-k)\sin\left(2\omega_g t+\theta^{-}+\rho\right)}^{q_{osc2}}$$

All the expressions presented in this section become equal to the corresponding ones from the previous section when the negative sequence component V^{-} is equal to 0. The proposed control strategy accomplishes sinusoidal currents and maintains the same power factor on the grid side without changing the output characteristics of the converter.

5 | MAXIMUM CONVERTER VOLTAGE GAIN

By using the control strategy proposed in the previous section, the output voltage remains unchanged when unbalanced grid conditions occur. However, the maximum voltage gain of the converter is expected to decrease because input voltage unbalance is compensated on the load side. To keep the converter operating in the linear range, the following condition must be satisfied:

$$\left|\underline{m_{ccw}}\right|+\left|\underline{m_{cw}}\right|\le\frac{3}{2} \tag{47}$$

The following analysis aims to find the maximum modulation index m_{max} for which SVM is operating in the linear range. At the particular moment when $2\omega_g t=\pi-\theta^{-}-2\alpha$, the complex modulation indexes $\underline{m_{ccw}}$ (35) and $\underline{m_{cw}}$ (36) reach their maximum amplitude levels given by (48) for the set value of modulation index m.

$$\left|\underline{m_{ccw}}\right|_{max}^{I}=\left|\underline{m_{cw}}\right|_{max}^{I}=\frac{3}{4}m'(1+u) \tag{48}$$

Similarly, maximum amplitude levels of complex modulation indexes (49), which refer to method II, can be obtained by substituting $2\omega_g t=\pi-\theta^{-}$ into Equations (42) and (43).

$$\left|\underline{m_{ccw}}\right|_{max}^{II}=\frac{3}{2}m'k+\frac{3}{2}m'(1-k)u$$

$$\left|\underline{m_{cw}}\right|_{max}^{II}=\frac{3}{2}m'(1-k)+\frac{3}{2}m'ku \tag{49}$$

For both methods, the modulation index should be limited to m_{max} given by (50), which is obtained by substituting (48) or (49) into (47) and finding the boundary value of the linear operating range.

$$m_{max}=1-u \tag{50}$$

Voltage gain Equations (51) and (52) for methods I and II are derived from output voltage expressions (39) and (44). Its maximum values can be found simply by substituting modulation index m with its maximum value m_{max}, given by Equation (50).

$$q^{I}=\frac{\left|\underline{V_o}\right|}{V^{+}}=\frac{3}{2}m\cos\alpha\ \rightarrow\ q_{max}^{I}=\frac{3}{2}(1-u)\cos\alpha \tag{51}$$

$$q^{II}=\frac{\left|\underline{V_o}\right|}{V^{+}}=\frac{3}{2}m\ \rightarrow\ q_{max}^{II}=\frac{3}{2}(1-u) \tag{52}$$

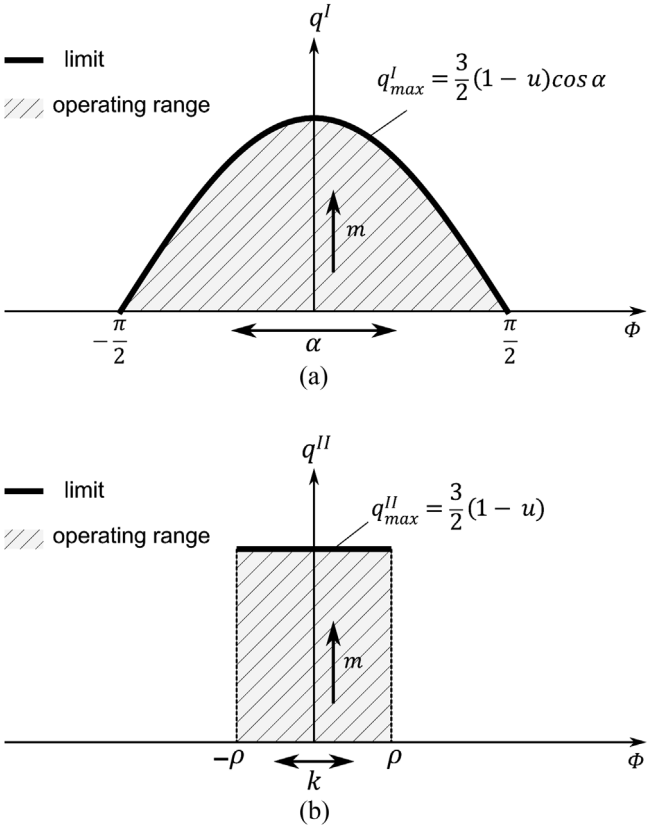

FIGURE 5 Linear operating range of the SVM and its limit under unbalanced grid conditions. **(a)** Method I, **(b)** method II. SVM, space-vector-modulation.

Based on previous analysis, graphics representing converter voltage gain dependence of grid power factor angle are presented in Figure 5. By using the method I input power factor can be controlled in any range $-\frac{\pi}{2} \le \Phi \le \frac{\pi}{2}$, but a maximum voltage gain q^I_{max} decreases with factor $\cos\Phi$. On the other hand, method II can control input power factor angle in a limited range $-\rho \le \Phi \le \rho$, but without sacrificing output voltage capability. In both cases, under unbalanced input conditions, maximum voltage gain decreases with factor $1-u$.

6 | EXPERIMENTAL RESULTS

A test setup is established (Figure 6) with National Instruments sbRIO 9606 embedded controller to validate the proposed methods. Its analog and digital IO pins are connected to Typhoon HIL 602+ (Hardware in the loop) device. The model implemented on HIL consists of two 3 × 3 MCs, one at each side of an open-end three-phase *R-L* load. One of two methods is used to control the input power factor and generate 18 PWM signals to control the matrix converter's bidirectional switches modelled on the HIL device. DDSRF PLL [44] is used to synchronize to the three-phase voltage source and extract the positive and negative sequence components. Amplitude and frequency of three-phase voltage source are: $V^+ = 230\sqrt{2}\ V$, $f_g = 50$ Hz. Values of passive load components are as follows: $R = 15\ \Omega$, $L = 50$ mH. The switching frequency is equal to 5 kHz. Modulation index and output frequency are set to $m = 0.5$ and $f_o = 25$ Hz. HIL SCADA software is used for capturing input/output voltage and current waveforms. As shown in Figure 6, star terminals are created using resistors $R_m = 20\ \text{k}\Omega$ at converter's output terminals. CMVs are measured between the star terminals and the ground. Obtained results are presented in Figure 7a. One can observe that both CMVs $v_{cmv1,2}$ equal zero during the output voltage modulation.

Considering input currents and output voltages pulsing character, averaged values over one switching period T_s are presented. Input instantaneous active and reactive power are calculated using averaged values of input currents. Input voltages (v_{abc}), input currents ($\overline{i_{abc}}$), output voltages ($\overline{v_{ABC}}$), output currents (i_{ABC}), and instantaneous power components (p, q) are presented in Figures 8–11. By setting $\alpha = 0$ (Method I) or $k = 0.5$ (Method II), a unity power factor on the input side can be achieved, regardless of the output power factor angle. Two methods result in identical expressions for complex modulation indexes at this operating point. Time-domain graphics with the corresponding frequency spectrum of the signals are presented in Figures 8 and 9, respectively. Under balanced grid conditions (Figures 8a, 9a), when $V^- = 0$ there are no unwanted components in either input or output currents. Instantaneous reactive power is constant and equal to zero. Regarding the power distribution among two MCs, average values of input currents $\overline{i_{abc1}}$ and $\overline{i_{abc2}}$ of each of the two MC (MC1 and MC2) are measured and presented in Figure 7b. Currents of MC1 $\overline{i_{abc1}}$ and MC2 $\overline{i_{abc2}}$ result in identical waveforms in the time domain, only shifted in phase by 180°. The RMS value of each current is 10.2 A. Input currents are sinusoidal $\overline{i_{abc}}$ and set to be in phase with the grid voltage. The RMS value of input currents i_{abc} is equal to 12.17 A per phase. One can observe from Figures 8b and 9b that negative sequence component (set to $V^- = 0.25\text{V}^+$) generates two unwanted components in the output voltages and currents, at $|f_o - 2f_g|$ and $|f_o + 2f_g|$ frequencies (75 and 125 Hz). At the same time, the third harmonic will appear in grid currents (150 Hz). The corresponding results are consistent with Equations (33) and (34), derived in Section 4. It is shown in Figures 8c and 9c that all unwanted components can be eliminated by using the control strategy proposed in Section 4, resulting in sinusoidal but unbalanced input currents and unchanged output characteristics of the converter compared to the balanced conditions. These results are consistent with Equations (39) and (40), for the specail case when $\alpha = 0$. Instantaneous active power is constant, while the average reactive power remains zero with a superimposed oscillating component at twice the grid frequency, as shown by Equation (41).

To verify the performance of the extended version of method I proposed in Section 4, the input power factor is tuned to $\frac{\sqrt{2}}{2}$ leading ($\alpha = \frac{\pi}{4}$) and switched to $\frac{\sqrt{2}}{2}$ lagging ($\alpha = -\frac{\pi}{4}$) at $t = 0.03$ s. First test is done under balanced grid conditions ($V^- = 0$). The transient period is captured and presented in Figure 10a. One can observe that the input power factor angle

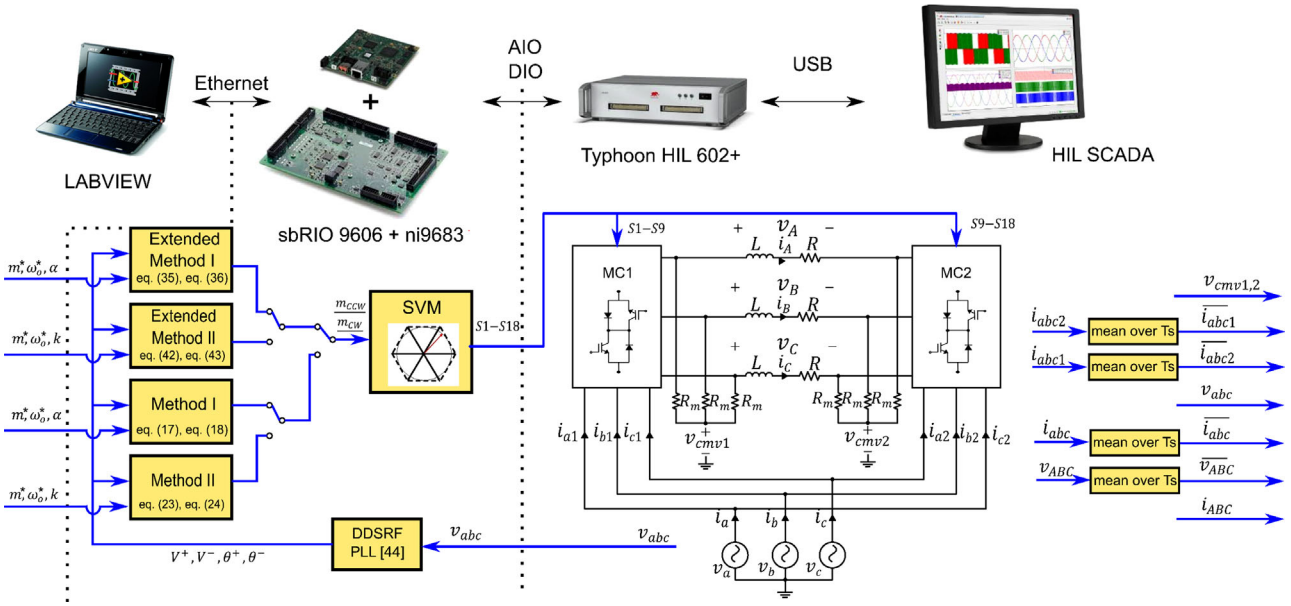

FIGURE 6 Block diagram of the real-time HIL test setup. HIL, hardware in the loop.

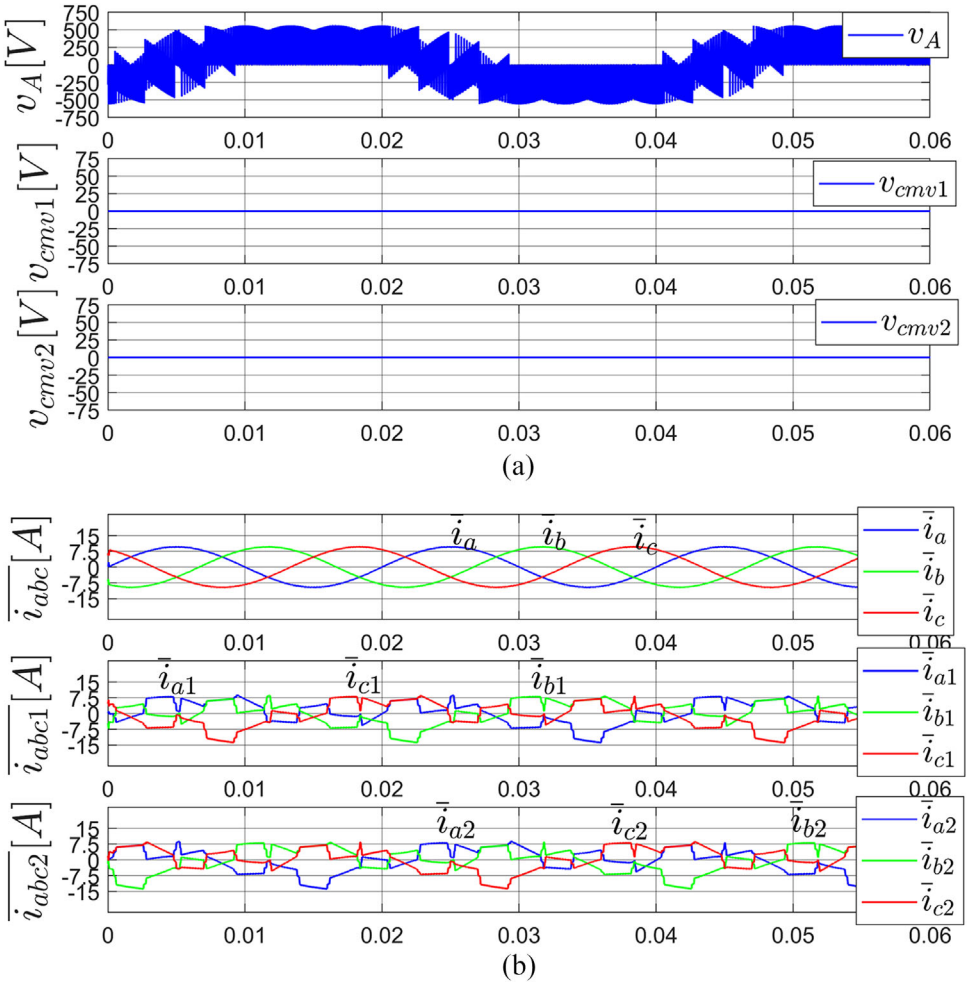

FIGURE 7 Experimental waveforms of (a) output phase A voltage v_A and measured common-mode voltages $v_{cmv1,2}$, (b) input currents $\overline{i_{abc}}$, input currents of MC1 $\overline{i_{abc1}}$ and input currents of MC2 $\overline{i_{abc2}}$. MC, matrix converters.

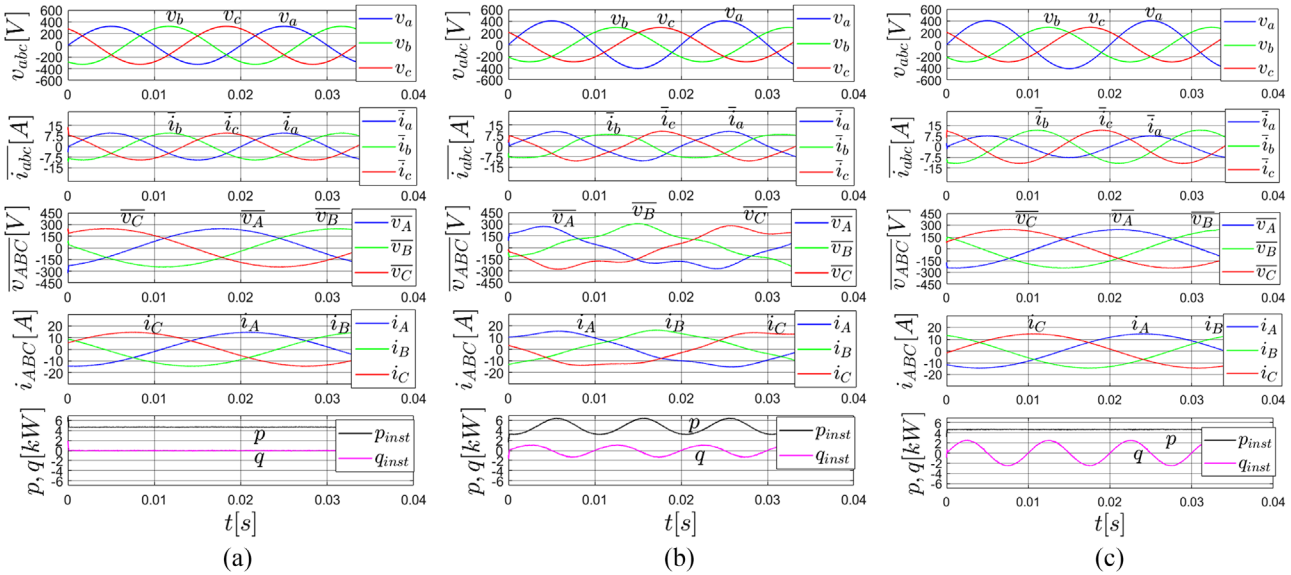

FIGURE 8 Time-domain graphs for unity power factor operation under (a) balanced input conditions ($V^- = 0$), (b) unbalanced input conditions without proposed control strategy ($V^- = 0.25V^+$), (c) unbalanced input conditions with proposed control strategy ($V^- = 0.25V^+$)

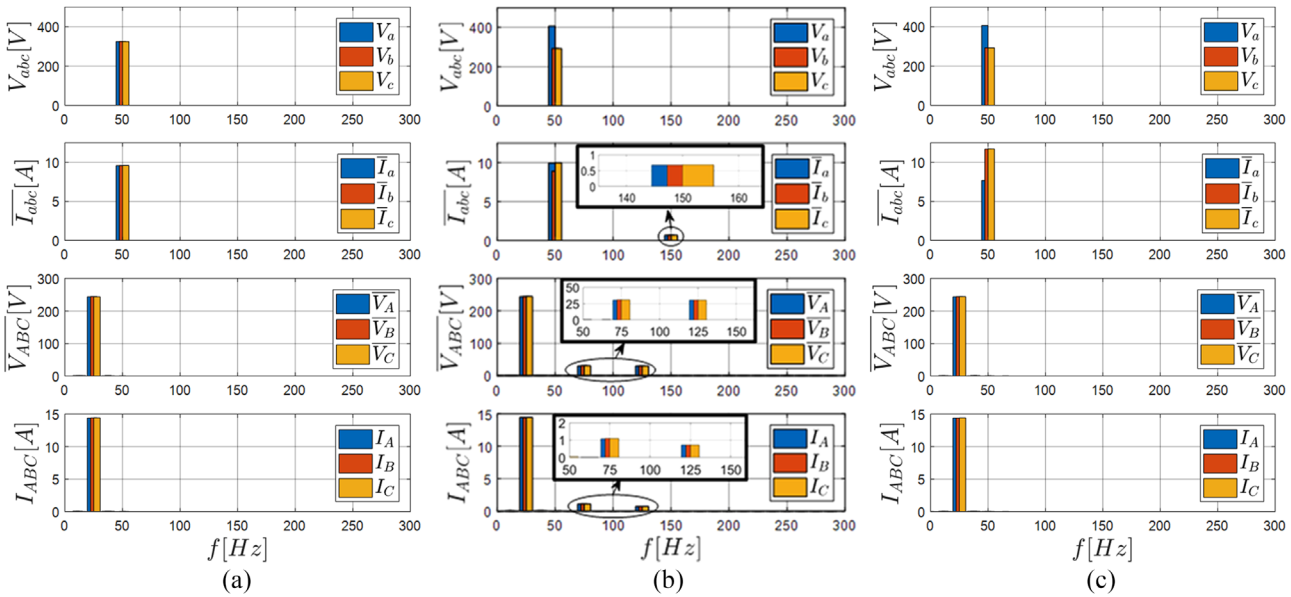

FIGURE 9 Frequency-domain graphs for unity power factor operation under (a) balanced input conditions ($V^- = 0$), (b) unbalanced input conditions without proposed control strategy ($V^- = 0.25V^+$), (c) unbalanced input conditions with proposed control strategy ($V^- = 0.25V^+$)

is equal to α, while output voltage decreases with $\cos\alpha$, as expected by Equations (39) and (40). The same test is done under unbalanced conditions ($V^- = 0.25\ V^+$) and the captured time diagrams are presented in Figure 10b. Compared to balanced grid conditions, the difference is the existence of negative sequence component in the grid current at the fundamental frequency and an oscillating component of reactive grid power. Also, the dc value of grid reactive power is slightly higher due to factor γ, defined by Equation (41). The extended version of method II is tested for two boundary values of coefficient k: $k = 0$ and $k = 1$. The input power factor is set to $\cos\rho = 0.886$ leading ($k = 0$) and switched to $\cos\rho = 0.886$lagging ($k = 1$) at $t = 0.03$ s. The transient period is captured under balanced and unbalanced grid conditions, and the obtained results are presented in Figures 11a and 11b. Unlike method I, there is no reduction in output voltage capability, as predicted by Equation (44). On the other hand, the power factor angle is limited to $\cos\rho$. Other than that, the same conclusions drawn by testing method I can be applied here.

The results obtained by the HIL test setup present the average value of input currents over one switching period. Such representation neglects the high-frequency component at the

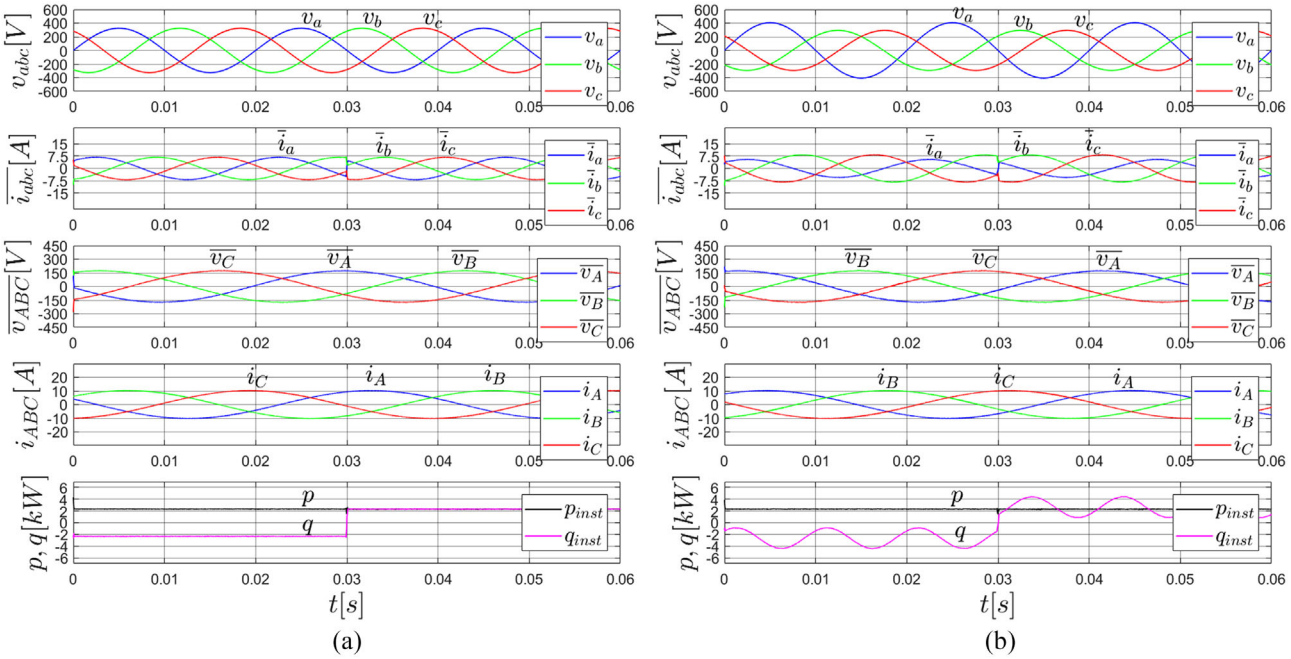

FIGURE 10 Performance verification for extended version of method I during step change from $\alpha = \frac{\pi}{4}$ to $\alpha = -\frac{\pi}{4}$ under (a) balanced input conditions ($V^- = 0$), (b) unbalanced input conditions ($V^- = 0.25V^+$)

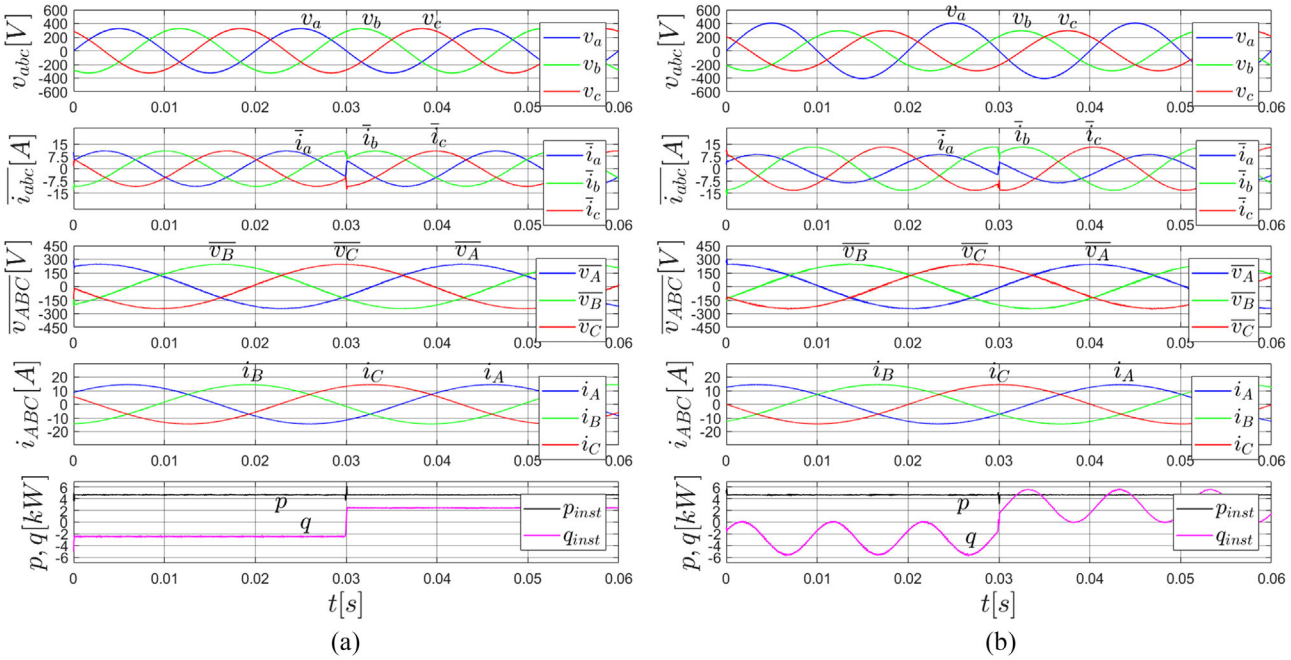

FIGURE 11 Performance verification for extended version of method II during step change from $k = 0(\Phi = \rho)$ to $k = 1(\Phi = -\rho)$ under (a) balanced input conditions ($V^- = 0$), (b) unbalanced input conditions ($V^- = 0.25V^+$)

switching frequency and its harmonics, with negligible influence on the low-frequency components. The input filter would be used in the actual experiment, which should provide the required attenuation of the high-frequency harmonics with minimal influence on the fundamental low-frequency components of the input currents.

7 | CONCLUSION

This paper investigates two grid power factor control methods for direct-matrix-converter-based drive supplied by unbalanced grid. Both methods are based on the SVM technique that uses only rotating voltage vectors to control output voltages and grid

power factor angle while eliminating high-frequency CMV at the output terminals. A novel converter model, written in a complex form, has been proposed and used for analysis. It has been shown that two methods differ in the range in which grid power factor angle can be controlled, as well as output voltage capability. Furthermore, new extended versions of both methods have been proposed to improve the converter's performance under unbalanced grid conditions. Both the proposed control methods obtain sinusoidal grid currents while maintaining reactive power control. On the load side, the waveform quality of the output currents remains unchanged. Finally, the experimental results obtained on the HIL laboratory setup verified the previous theoretical analysis and the effectiveness of the proposed control strategy even in the presence of high grid voltage unbalances of 25%.

AUTHOR CONTRIBUTIONS

Luka Stanić: Conceptualization; Data curation; Formal analysis; Investigation; Methodology; Resources; Software; Validation; Visualization; Writing – original draft. Leposava Ristić: Conceptualization; Funding acquisition; Investigation; Methodology; Project administration; Resources; Supervision; Validation; Writing – review & editing. Milan Bebić: Conceptualization; Formal analysis; Investigation; Methodology; Resources; Supervision; Validation; Visualization; Writing – review & editing. Marco Rivera: Funding acquisition; Investigation; Project administration; Resources; Supervision; Validation; Visualization; Writing – review & editing.

ACKNOWLEDGEMENTS

The authors of this paper would like to thank Typhoon HIL, Inc.® for their help and support. This paper was created during research funded by Ministry of Education, Science and Technological Development, Republic of Serbia grant no. 2022/200103, CLIMAT grant no. AMSUD210001 and Fondecyt Regular grant no. 1220556.

CONFLICT OF INTEREST

The authors have declared no conflict of interest.

DATA AVAILABILITY STATEMENT

The data that support the findings of this study are available from the corresponding author upon reasonable request.

REFERENCES

1. Buticchi, G., Bozhko, S., Liserre, M., Wheeler, P., Al-Haddad, K.: On-board microgrids for the more electric aircraft—Technology review. IEEE Trans. Ind. Electron. 66(7), 5588–5599 (2019)
2. Mir, T.N., Singh, B., Bhat, A.H.: FS-MPC-based speed sensorless control of matrix converter fed induction motor drive with zero common mode voltage. IEEE Trans. Ind. Electron. 68(10), 9185–9195 (2021)
3. Zhang, J., Yang, H., Wang, T., Li, L., Dorrell, D.G., Lu, D.D.-C.: Field-oriented control based on hysteresis band current controller for a permanent magnet synchronous motor driven by a direct matrix converter. IET Power Electron. 11(7), 1277–1285 (2018)
4. Pinto, S.F., Alcaria, P., Monteiro, J., Silva, J.F.: Matrix converter-based active distribution transformer. IEEE Trans. Power Delivery 31(4), 1493–1501 (2016)
5. Toledo, S., Gregor, R., Rivera, M., et al.: Multi-modular matrix converter topology applied to distributed generation systems. In 8th IET International Conference on Power Electronics, Machines and Drives (PEMD 2016), pp. 1–6 (2016)
6. Diaz, M., Cardenas, R., Espinoza, M., et al.: Control of wind energy conversion systems based on the modular multilevel matrix converter. IEEE Trans. Ind. Electron. 64(11), 8799–8810 (2017)
7. Monteiro, J., Silva, J.F., Pinto, S.F., Palma, J.: Matrix converter-based unified power-flow controllers: Advanced direct power control method. IEEE Trans. Power Delivery 26(1), 420–430 (2011)
8. Zhang, J.W., Dorrell, D.G., Li, L.: Applications of the direct space vector modulation controlled matrix converter as the unified power flow controller. In 8th IET International Conference on Power Electronics, Machines and Drives (PEMD 2016), pp. 1–6 (2016)
9. Rivera, M., Rodriguez, J., Espinoza, J.R., Abu-Rub, H.: Instantaneous reactive power minimization and current control for an indirect matrix converter under a distorted AC supply. IEEE Trans. Ind. Inf. 8(3), 482–490 (2012)
10. Rajendran, S., Govindarajan, U., Parvathi Sankar, D.S.: Active and reactive power regulation in grid connected wind energy systems with permanent magnet synchronous generator and matrix converter. IET Power Electron. 7(3), 591–603 (2014)
11. Hamouda, M., Blanchette, H.F., Al-Haddad, K.: Unity power factor operation of indirect matrix converter tied to unbalanced grid. IEEE Trans. Power Electron. 31(2), 1095–1107 (2016)
12. Mondal, S., Kastha, D.: Improved direct torque and reactive power control of a matrix-converter-fed grid-connected doubly fed induction generator. IEEE Trans. Ind. Electron. 62(12), 7590–7598 (2015)
13. Malekjamshidi, Z., Jafari, M., Zhu, J., Xiao, D.: Comparative analysis of input power factor control techniques in matrix converters based on model predictive and space vector control schemes. IEEE Access 7, 139150–139160 (2019)
14. Huber, L., Borojevic, D.: Space vector modulated three-phase to three-phase matrix converter with input power factor correction. IEEE Trans. Ind. Appl. 31(6), 1234–1246 (1995)
15. Lei, J., Feng, S., Zhou, B., Nguyen, H.-N., Zhao, J., Chen, W.: A simple modulation scheme with zero common-mode voltage and improved efficiency for direct matrix converter-fed PMSM drives. IEEE J. Emerg. Select. Topics Power Electron. 8(4), 3712–3722 (2020)
16. Gupta, R.K., Mohapatra, K.K., Somani, A., Mohan, N.: Direct-matrix-converter-based drive for a three-phase open-end-winding AC machine with advanced features. IEEE Trans. Ind. Electron. 57(12), 4032–4042 (2010)
17. Hojabri, H., Mokhtari, H., Chang, L.: Reactive power control of permanent-magnet synchronous wind generator with matrix converter. IEEE Trans. Power Delivery 28(2), 575–584 (2013)
18. Li, X., Su, M., Sun, Y., Dan, H., Xiong, W.: Modulation strategy based on mathematical construction for matrix converter extending the input reactive power range. IEEE Trans. Power Electron. 29(2), 654–664 (2014)
19. Szczepankowski, P.: An extended control of the input angle for matrix converters connected with the non-unity power factor loads. IEEE Trans. Ind. Electron. 69(12), 12009–12018 (2021)
20. Casadei, D., Serra, G., Tani, A.: Reduction of the input current harmonic content in matrix converters under input/output unbalance. IEEE Trans. Ind. Electron. 45(3), 401–411 (1998)
21. Blaabjerg, F., Casadei, D., Klumpner, C., Matteini, M.: Comparison of two current modulation strategies for matrix converters under unbalanced input voltage conditions. IEEE Trans. Ind. Electron. 49(2), 289–296 (2002)
22. Stanić, L., Ristić, L., Bebić, M., Rivera, M.: Extended SVM for direct matrix converter based drive operating under unbalanced grid conditions. In: 2021 21st International Symposium on Power Electronics (Ee), pp. 1–6 (2021)
23. Wang, X., Lin, H., She, H., Feng, B.: A research on space vector modulation strategy for matrix converter under abnormal input-voltage conditions. IEEE Trans. Ind. Electron. 59(1), 93–104 (2012)

24. Dasika, J.D., Saeedifard, M.: An online modulation strategy to control the matrix converter under unbalanced input conditions. IEEE Trans. Power Electron. 30(8), 4423–4436 (2015)
25. Li, X., Su, M., Sun, Y., Dan, H., Xiong, W.: Modulation strategies based on mathematical construction method for matrix converter under unbalanced input voltages. IET Power Electron. 6(3), 434–445 (2013)
26. Lei, J., Zhou, B., Bian, J., Qin, X., Wei, J.: A simple method for sinusoidal input currents of matrix converter under unbalanced input voltages. IEEE Trans. Power Electron. 31(1), 21–25 (2016)
27. Feng, S., Lei, J., Zhao, J., Chen, W., Deng, F.: Improved reference generation of active and reactive power for matrix converter with model predictive control under input disturbances. IEEE Access 7, 97001–97012 (2019)
28. Xiong, W., Sun, Y., Lin, J., et al.: A cost-effective and low-complexity predictive control for matrix converters under unbalanced grid voltage conditions. IEEE Access 7, 43895–43905 (2019)
29. Lei, J., Zhou, B., Bian, J., et al.: Feedback control strategy to eliminate the input current harmonics of matrix converter under unbalanced input voltages. IEEE Trans. Power Electron. 32(1), 878–888 (2017)
30. Gontijo, G.F., Tricarico, T.C., França, B.W., da Silva, L.F., van Emmerik, E.L., Aredes, M.: Robust model predictive rotor current control of a DFIG connected to a distorted and unbalanced grid driven by a direct matrix converter. IEEE Trans. Sustain. Energy 10(3), 1380–1392 (2019)
31. Rodriguez, J., Rivera, M., Kolar, J.W., Wheeler, P.W.: A review of control and modulation methods for matrix converters. IEEE Trans. Ind. Electron. 59(1), 58–70, (2012)
32. Kalaiselvi, J., Srinivas, S.: Bearing currents and shaft voltage reduction in dual-inverter-fed open-end winding induction motor with reduced CMV PWM methods. IEEE Trans. Ind. Electron. 62(1), 144–152 (2015)
33. Somani, A., Gupta, R.K., Mohapatra, K.K., Mohan, N.: On the causes of circulating currents in PWM drives with open-end winding AC machines. IEEE Trans. Ind. Electron. 60(9), 3670–3678 (2013)
34. Alesina, A., Venturini, M.G.B.: Analysis and design of optimum-amplitude nine-switch direct AC-AC converters. IEEE Trans. Power Electron. 4(1), 101–112 (1989)
35. Xiong, W., Sun, Y., Su, M., Yang, J., Wang, C.: A carrier-based modulation strategy for multi-modular matrix converters with zero common-mode voltage. In 2016 IEEE Energy Conversion Congress and Exposition (ECCE), pp. 1–6 (2016)
36. Nguyen, H.-N., Lee, H.-H.: An enhanced SVM method to drive matrix converters for zero common-mode voltage. IEEE Trans. Power Electron. 30(4), 1788–1792 (2015)
37. Wang, L., Dan, H., Zhao, Y., et al.: A finite control set model predictive control method for matrix converter with zero common-mode voltage. IEEE J. Emerg. Select. Topics Power Electron. 6(1), 327–338 (2018)
38. Nguyen, H.-N., Lee, H.-H.: A modulation scheme for matrix converters with perfect zero common-mode voltage. IEEE Trans. Power Electron. 31(8), 5411–5422 (2016)
39. Arioni, A.D., Padilha, T.S., Oliveira, S.V.G.: Expanded space vector modulation of direct matrix converters including hidden rotating pairs. IEEE Trans. Ind. Electron. 66(11), 8296–8307 (2019)
40. Rząsa, J.: An alternative carrier-based implementation of space vector modulation to eliminate common mode voltage in a multilevel matrix converter. Electronics 8(2), 190 (2019)
41. Deng, W.: Maximum voltage transfer ratio of matrix converter under DTC with rotating vectors. IEEE Trans. Power Electron. 36(6), 6137–6141 (2021)
42. Mohapatra, K.K., Mohan, N.: Open-end winding induction motor driven with matrix converter for common-mode elimination. In: 2006 International Conference on Power Electronic, Drives and Energy Systems, pp. 1–6 (2006)
43. Tewari, S., Mohan, N.: Matrix converter based open-end winding drives with common-mode elimination: topologies, analysis, and comparison. IEEE Trans. Power Electron. 33(10), 8578–8595 (2018)
44. Rodriguez, P., Pou, J., Bergas, J., Candela, J.I., Burgos, R.P., Boroyevich, D.: Decoupled double synchronous reference frame PLL for power converters control. IEEE Trans. Power Electron. 22(2), 584–592 (2007)

How to cite this article: Stanić, L., Ristić, L., Bebić, M., Rivera, M.: Improvement of two grid power factor control methods for matrix converter open-end-winding drive with common-mode voltage elimination supplied by unbalanced grid. IET Power Electron. 1–16 (2022). https://doi.org/10.1049/pel2.12411